Magnetic Behavior of Heterometallic Wheels Having a [MnIV6M2O9]10+Core with M = Ca2+ and Sr2+

Luis Escriche-Tur, [*,†] Jesús Jover, [†] Mercè Font-Bardia, [‡] Gabriel Aullón, [†,§] and Montserrat Corbella [*,†,∥]

†Departament de Química Inorgànica and ‡Cristal·lografia, Mineralogia i Dipòsits Minerals, Universitat de Barcelona, Barcelona 08028, Spain
§Institut de Química Teòrica i Computacional de la Universitat de Barcelona (IQTCUB), Barcelona 08028, Spain
∥Institut de Nanociencia i Nanotecnologia de la Universitat de Barcelona (IN2UB), Barcelona 08028, Spain

ABSTRACT

Two new heterometallic MnIV−M2+ compounds with formula [Mn6M2O9(4-tBuC6H4COO)10(4-tBuC6H4COOH)5] (M = Ca2+ (1), Sr2+ (2)) have been crystallized. The core of both compounds consists of a planar Mn6 ring, where the MnIV ions are alternatively bridged by (μ3-O)2(μ-RCOO) and (μ4-O)(μ-RCOO)2 ligands, and the two alkaline earth ions are located to both sides of the wheel, linked to the oxo bridges, generating three fused [Mn2M2O4]4+ cuboids. These compounds show a net antiferromagnetic behavior, more important for 2 (Sr2+) than for 1 (Ca2+). The fitting of the experimental data was performed with the support of DFT calculations, considering four different exchange pathways: two between adjacent MnIV ions (J1 and J2) and two between nonadjacent MnIV ions (J3 and J4). The results of the analysis show that J1 and J2 are of the opposite sign, the ferromagnetic contribution corresponding to the [Mn2(μ4-O)(μ-RCOO)2]4+ unit (J2). The influence of the M2+ ions in the magnetic behavior is analyzed for 1 and 2 and for three hypothetical models with the structural parameters of 1 containing Mg2+, Sr2+ or without the M2+ ions. In spite of the diamagnetic character of the alkaline earth ions, their influence on the magnetic behavior has been evidenced and correlated with their polarizing effect. Moreover, the magnetic interactions between nonadjacent ions are non-negligible.

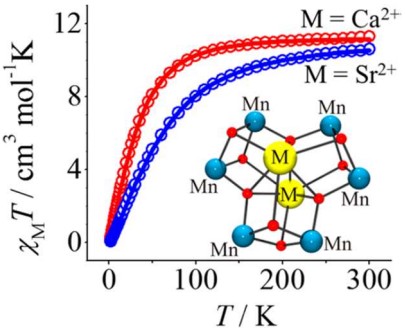

INTRODUCTION

High oxidation state Mn compounds are of relevance to a large number of areas and applications due to their ability to oxidize both inorganic and organic substrates.[1,2] Moreover, there are many metalloproteins involving one or more Mn ions in enzymatic functions. Particularly, a heterometallic [Mn4CaO5] cubane-like cluster constitutes the water-oxidizing center (WOC) within photosystem II (PSII), a membrane-bound protein that performs the light-induced oxidation of H_2O to O_2, being responsible for the production of a great part of the atmospheric oxygen on Earth and the fixation of carbon dioxide.[3,4] In the proposed catalytic cycle (known as the Kok cycle), a four-electron oxidation of two H_2O molecules takes place in five intermediate Si states (i = 0−4) in which the Mn oxidation state mainly swings between III and IV and some structural changes may be observed in the coordination environment of the Mn ions.[5−8] Searching for synthetic analogues, a huge number of manganese clusters may be found in the literature, including homo-9 and heterometallic Mn−Ca[10−19] compounds. However, only three compounds with a $[Mn^{IV}_3CaO_4]^{6+}$ cubane-like core have been reported.[17,18,20]

In spite of the researchers' efforts, electronic changes in the WOC still remain incompletely understood. Furthermore, Ca^{2+} ion plays a crucial role in oxygen evolution because alkali or lanthanide substitution or Ca^{2+} depletion resulted in the inhibition or worsening of the catalytic process.[21] It also has an influence on the geometrical and electronic structure of the WOC (related to the electron and proton transfer)[22] and maintains the correct configuration of the surrounding network of water molecules, contrary to other metal ions.[23] These facts suggest that Ca^{2+} ion is neither replaceable nor dispensable. Moreover, data comparison between the Si states and a series of MnIV compounds revealed that the Ca^{2+} ion is apparently modifying the electronic structure of the Mn ions, also suggesting that the assignment of formal oxidation states is insufficient for accurately understanding the electronic structural changes of Mn.[24]

Sr^{2+} has been considered a good candidate for replacing Ca^{2+} in the majority of the systems, even though the latter is significantly smaller (ionic radii of 1.14 Å for Ca^{2+} and 1.32 Å for Sr^{2+}). For instance, they show very similar activities in O_2 chemistry due to their similarities generating H-bonding networks.[25] Mn−Sr^{2+} and Mn−Ca^{2+} compounds also display very similar redox potentials, a fact that seems to be related to the similarity between their acidities←in comparison to other Mn−Mz′ compounds.[19,26] Consistently, the Sr^{2+}-substituted PSII is active toward H_2O oxidation, while substitution of the Ca^{2+} ion (in the native site) for other cations or Ca^{2+} depletion results in the inhibition of the activity. Some of these cations, such as Cd^{2+}, Cu^{2+}, and Dy^{3+}, may fulfill the structural role of Ca^{2+}, but they are not able to provide the required electronic modifications. This fact seems to be related to the functional role of Ca^{2+} to activate H_2O, which can be partially fulfilled with a cation with similar Lewis acidity, such as Sr^{2+}.[21,27,28] However, the Sr^{2+} substitution is not innocent, because it causes some obvious structural changes in the WOC[29,30] and negatively affects the kinetics of H_2O oxidation.[31]

We herein present the synthesis and crystal structure of two wheels with formula $[Mn_6M_2O_9(4\text{-}tBuC_6H_4COO)_{10}(4\text{-}tBuC_6\text{-}H_4COOH)_5]$, where M = Ca^{2+} (1) or Sr^{2+} (2). Several compounds with a Mn6 wheel-like core have been reported in the literature, showing a wide range of combinations of Mn oxidation states and central ions.[32−46] These wheels can be classified in two types: (a) those where the Mn ions are linked through two oxo or oxo derivatives and (b) those where the Mn ions are alternately bridged through one and two oxo or oxo derivatives. Type a wheels prove the versatility of these compounds, which include several Mnz 6Mz′x moieties, where z is the Mn oxidation state, Mz′ is the central ion with the z′ oxidation state, and x is 1 or 2. Then these wheels include the compounds with Mn^{II} 6Mn^{II},[32] Mn^{III}_6Na,[41,42] and Mn^{III}_6Li moieties[40] and several mixed-valence compounds with $Mn^{II/III}_6Mn^{II}$ moieties.[33−39] In contrast, most of type b wheels are compounds with

MnIV6CeIVx44,45 and MnIV6BiIII2 moieties;46 only one MnIII6MnII wheel has been described.43 All these compounds are of great interest for inorganic chemists due to their magnetic properties. For instance, a lot of them present a net ferromagnetic behavior, and some are single-molecule magnets (SMM) at low temperature.36,39,43

Among the three MnIV 6Mz′x wheels, magnetic analysis is only reported for the CeIV compounds. Here, we also report the study of the magnetic properties of the new MnIV 6 wheels (with Ca2+ and Sr2+). With the aim to elucidate the effect of the alkaline earth ions on the magnetic properties, DFT calculations have been performed for compounds 1 (Ca2+) and 2 (Sr2+) and for three hypothetical compounds with the structural parameters of 1 (where Ca2+ has been replaced with Sr2+, Mg2+, or M2+ depletion).

EXPERIMENTAL SECTION

Synthesis. All manipulations were performed under aerobic conditions. NBu_4MnO_4 was prepared as described in the literature.47

$[Mn_6Ca_2O_9(4\text{-}tBuC_6H_4COO)_{10}(4\text{-}tBuC_6H_4COOH)_5]$ (1). A mixture of $Mn(CH_3COO)_2{\cdot}4H_2O$ (0.25 mmol, 0.060 g), 4-$tBuC_6H_4COOH$ (8.2 mmol, 1.46 g), and $Ca(NO_3)_2{\cdot}xH_2O$ (0.25 mmol, 0.060 g) was dissolved in CH_3CN (60 mL) and then heated up to 80 °C. The resulting orange solution was softly stirred for 15 min, while solid NBu_4MnO_4 (0.5 mmol, 0.18 g) was added in small portions. The dark red solution was allowed to cool at room temperature and filtered with the aim to separate any possible solid residue. After 2 or 3 days of slow evaporation, dark red crystals were collected by filtration, washed with EtOH, and dried under vacuum. Yield (based on total Mn): 60%. Anal. Calcd for $C_{165}H_{200}Ca_2Mn_6O_{39}{\cdot}0.25\ CH_3CN$ (MW = 3227 g mol−1): C, 61.59; H, 6.27; N, 0.11; Mn, 10.21; Ca, 2.48. Found: C, 58.94; H, 6.39; N, 0.11; Mn, 10.49; Ca, 2.24. Selected IR data (cm−1): 3427 (br), 2964 (m), 2905 (w), 2869 (w), 1691 (m), 1610 (m), 1587 (m), 1541 (m), 1501 (w), 1462 (w), 1400 (s), 1315 (w), 1268 (m), 1194 (m), 1107 (w), 855 (w), 780 (m), 750 (w), 726 (m), 710 (m), 630 (m), 526 (w).

This compound may also be synthesized using $Ca(CH_3COO)_2{\cdot}\ xH_2O$ (0.25 mmol, 0.040 g) as the calcium source instead of $Ca(NO_3)_2{\cdot}xH_2O$. Unlike the procedure previously described, a white suspension appeared before addition of NBu_4MnO_4, identified by IR spectroscopy as Mn(4-$tBuC_6H_4COO)_2$. After cooling, the solution was filtered to separate the surplus $Ca(CH_3COO)_2$. After a week of slow evaporation, dark red crystals were collected by filtration, washed with EtOH, and dried under vacuum. Yield (based on total Mn): 10%.

Both synthetic routes lead to the crystallization of 1, providing single crystals from the mother liquor. The crystals obtained using $Ca(NO_3)_2$ were very small, and even though we could determine the cell parameters and isotropically refine all atoms, we were unable to finish the refinement of the crystal structure. In contrast, crystals obtained using $Ca(CH_3COO)_2$ were highly diffracting, and we could successfully refine the crystal structure.

The molar conductivity (ΛM) of compound 1 is 1.6 S cm2 mol−1 in CH_2Cl_2 solution and 23 S cm2 mol−1 in CH_3CN solution (the expected values for a 1:1 electrolyte are 10−24 S cm2 mol−1 in CH_2Cl_2 and 120−160 S cm2 mol−1 in CH_3CN).48 These values are in agreement with a neutral compound.

$[Mn_6Sr_2O_9(4\text{-}tBuC_6H_4COO)_{10}(4\text{-}tBuC_6H_4COOH)_5]$ (2). An analogous procedure was followed as for 1 but using $Sr(NO_3)_2$ (0.25 mmol, 0.053 g) and only 40 mL of CH_3CN. After 1 or 2 days, dark red crystals were collected by filtration, washed with EtOH, and dried under vacuum. Yield (based on total Mn): 7%. Single crystals suitable for X-ray analysis were obtained from the mother liquor. Anal. Calcd for $C_{165}H_{200}Mn_6O_{39}Sr_2{\cdot}0.20\ CH_3CN$ (MW = 3320 g mol−1): C, 59.83; H, 6.09; N, 0.08. Found: C, 58.02; H, 6.31; N, 0.08. Selected IR data (cm−1): 3443 (br), 2964 (m), 2898 (w), 2869 (w), 1691 (m), 1611 (m), 1586 (m), 1540 (m), 1501 (w), 1462 (w), 1398 (s), 1315 (w), 1268 (m), 1193 (m), 1107 (w), 855 (w), 782 (m), 750 (w), 726 (m), 710 (m), 625 (m), 526 (w).

X-ray Crystallography. Crystallographic data collection and structure refinement details for 1 and 2 are summarized in Table S1. The data collection was performed at 100 K on a Bruker Apex-II diffractometer with graphite-monochromated Mo Kα radiation (λ = 0.71073 Å). Unit-cell parameters were determined from ~9700 reflections (~2.30° < θ < ~25.5°) and refined by least-squares method. There were 228 289 reflections (2.09° < θ < 25.10°) for 1 and 84 790 reflections (2.08° < θ < 26.39°) for 2 collected using the Φ- and ω-scan method. The data were corrected for absorption effects using the multiscan method (SADABS).49

The structures were solved by direct methods and refined by fullmatrix least-squares using SHELXL-97.50 Non-hydrogen atoms were refined anisotropically, whereas hydrogen atoms were computed and refined with isotropic thermal parameters riding on their respective carbon or oxygen atoms.

Both compounds crystallize in hexagonal space group P63/m. Their asymmetric unit consists of a sixth part of the [Mn6M2O9]10+ cluster (M = Ca2+ for 1 and Sr2+ for 2) with two nonequivalent Mn ions placed on a mirror plane and one M2+ ion placed on a 3-fold axis. The entire cluster is generated by these two last symmetry operators. The space between clusters is filled by acetonitrile molecules. No counteranion was found. One of the hydrogen atoms was computed with 5/6 (83.33%) overall occupancy to balance the charge of the [Mn6M2O9]10+ core, consistent with five hydrogen atoms delocalized in six identical positions (explanation in the Results and Discussion). A total of 376 parameters were refined in the final cycle of refinement on F2 using five restraints.

As commented before, 1 may be obtained using calcium nitrate or acetate. Single crystals obtained from both calcium sources were isolated and mounted on the diffractometer, the cell parameters of both crystals being practically identical. However, the crystal structure obtained via calcium nitrate could not be fully refined because the solvent molecules made the refinement unstable (due to the lack of reflections). On the other hand, the synthesis with calcium acetate provided bigger single crystals, whose crystal structure could be fully refined. Hence, the results presented before correspond to crystals obtained from the calcium acetate.

Structural Analysis. Experimental structural data were retrieved from the Cambridge Structural Database (WebCSD v1.1.1 updated in July 22, 2015). A search for structures with six almost coplanar Mn ions linked through oxygen atoms and with a minimum one ion in the center (bound at least to three of the oxygen atoms) was performed, finding a total of 20 different structures.

Physical Measurements. C, H, and N analysis were performed by the "Centres Cientifi cs i Tecnologì ics" of the Universitat de Barcelona. Mn and Ca semiquantitative analysis for 1 was performed with inductively coupled plasma optical emission spectrometry (ICP-OES) by the "Centres Cientifí cs i Tecnologì ics" of the Universitat de Barcelona from a solution of 1 (∼5 mg) pretreated in hot HNO3. Infrared spectra were recorded on KBr pellets in the 4000−400 cm−1 range with a Thermo Nicolet Avatar 330 FTIR spectrometer. Magnetic susceptibility measurements (2−300 K) for 1 and 2 were carried out in a Quantum Design MPMS XL5 SQUID Magnometer at the Unitat de Mesures Magnètiques (Universitat de Barcelona). Two different magnetic fields were used for the susceptibility measurements, 200 (2−29 K) and 3000 G (2−300 K), with imposable graphs. Pascal's constants were used to estimate the diamagnetic corrections for both compounds. The fit of the magnetic susceptibility was performed minimizing the function $R = \Sigma[(\chi MT)exp - (\chi MT)calcd]2/\Sigma[(\chi MT)exp]2$. The ionic conductivity measurements were made on 1 mM solutions of 1 in CH2Cl2 and in CH3CN using a CDC401 electrode.

Computational Details. Calculations were performed using the SIESTA code (Spanish Initiative for Electronic Simulations with Thousands of Atoms).51 The generalized-gradient functional proposed by Perdew, Burke, and Ernzerhof (PBE) was used.52 Only valence electrons were included in the calculations, with the core electrons being replaced by norm-conserving scalar relativistic pseudopotentials factorized in the Kleinman−Bylander form,53 generated according to the procedure of Trouiller and Martins.54 In the calculations, values of 50 meV for the energy shift and 250 Ry for the mesh cutoff were employed because they provide a good compromise between accuracy and computer time to estimate exchange coupling constants.

The crystal structures of compounds 1 and 2 were used for the calculations, keeping the experimental symmetry in which all six manganese ions are equivalent. The tBu substituents (on the aromatic ring) were simplified to methyl groups in order to optimize the computational resources. The broken-symmetry approximation without spin projection was employed, considering the spin Hamiltonian

mentioned in the text.55−57 The same calculations were also performed for three hypothetical compounds with Sr2+ and Mg2+ or without central ions. Aiming to preserve the structural parameters, the frozen symmetry of 1 was used for these hypothetical compounds, following the methodology reported by Ruiz et al.58−60 To calculate the exchange coupling constants (J), the energies for a high-spin state (where the six manganese spins are aligned in parallel, hence S = 9) and different low-spin solutions were computed (see Supporting Information). Four exchange pathways were considered from these energies to obtain their J values.

RESULTS AND DISCUSSION

Synthesis of [MnIV6M2O9(4-tBuC6H4COO)10(4-tBuC6-H4COOH)5] (M = Ca2+ for 1, and M = Sr2+ for 2). We synthesized two heterometallic compounds from the comproportionation reaction between Mn(AcO)2 and NBu4MnO4 in the presence of a M2+ salt and 4-tert-butylbenzoic acid (4-tBuC6H4COOH) in hot acetonitrile, procedure inspired by that described by Mukherjee et al. for the synthesis of an asymmetric [MnIV3CaO4]6+ cubane.18 Scheme 1 shows a concise synopsis of the reactions performed and some experimental observations. In our case, the use of Ca2+ acetate or nitrate leads to the formation of 1, in which the latter provides much higher yield. We also tested the same procedure using magnesium and strontium nitrate. While all attempts to obtain the analogous compound with Mg2+ ion were unsuccessful, the use of the Sr2+ source leads to the formation of 2. However, the synthesis of 2 hardly yielded 10% of the theoretical amount based on total Mn in spite of our endeavors. In all reactions, an excess of 4-tBuC6H4COOH was used, which may be required to favor the protonation of the acetate ions. The resulting acetic acid is very likely removed because of the high temperature.

The MnII/MnVII molar ratio (1:2) gives an oxidation state of +5.33 for each manganese ion. If all MnIV came from the comproportionation between MnII and MnVII, more than onehalf of the MnVII would be wasted. However, as the amount of 1 obtained exceeds the theoretical value based on this reaction, what occurs is that the comproportionation reaction is combined with the reduction of MnVII in the synthesis (at least for 1).

As commented before, 1 may be obtained using two different calcium sources: calcium nitrate and calcium acetate. The use of the last one leads to good X-ray-quality crystals, but the yield of the reaction is low. On the contrary, the use of calcium nitrate leads to the crystallization of 1 in a 60% yield; however, the obtained single crystals were too small, and the structure could not be fully refined. Although both synthetic routes lead to the formation of 1, a significant difference is observed in the first stage, which consists in the dissolution of MnII and Ca2+sources and 4-tBuC6H4COOH in hot acetonitrile. If calcium nitrate is used, the solution turns orange at 70 °C, indicating that part of the MnII is being oxidized to MnIII. In contrast, a white suspension, identified as Mn(4-tBuC6H4COO)2, appears at the same temperature when using calcium acetate. On the contrary, the solution does not turn orange during the first stage when using Sr(NO3)2 (synthesis of 2), indicating that there is no oxidation to MnIII. In all cases, the solution turns dark red after the addition of MnO4 −, which corresponds to the MnIV compound.

Particularly for 1, the crystal size is very sensitive to the stirring intensity, especially if calcium nitrate is chosen as the calcium source. If the solution is vigorously stirred during the addition of NBu4MnO4, a dark red powder is obtained just after the reaction, whereas if it is softly stirred, the isolated solid is crystalline. This confirms that 1 is instantly formed, and because of its insolubility in acetonitrile, the stirring induces a fast precipitation instead of a slow crystallization.

Description of Structures. 1 and 2, with formula [MnIV6M2O9(4-tBuC6H4COO)10(4-BuC6H4COOH)5] (M = Ca2+ for 1, and Sr2+ for 2), display very similar structures that mainly differ in the M2+ ions. Figure 1 shows the crystal structure of 1; the analogous picture of 2 is shown in Supporting Information (Figure S1).

These compounds contain a [MnIV6M2O9]10+ core which comprises a planar MnIV6 ring where the Mn ions are alternately bridged by (μ3-O)2(μ-RCOO) and (μ4-O)(μ-RCOO)2 ligands. The two M2+ ions are located in the center and at both sides of the wheel (Figures 2 and S2). The μ3-O ligand (O1) binds two Mn ions and the M2+ ion placed in the same side of the wheel, while the μ4-O ligand (O2) is linked to two Mn ions and the two M2+ ions, as shown in Figure 3.

In both compounds, the M2+ ions are located above and below the MnIV6 plane (at 1.83−1.90 Å from it) and linked to the oxo ligands, generating three fused [Mn2M2O4]4+ cuboids (Figure 3). The coordination number of these ions is nine; six of the positions are occupied by 3 μ3-O2− bridges (O1) and 3μ4-O2− bridges (O2). Each M2+ ion completes its coordination with three monodentate carboxylate ligands (Figure S3). The presence of hydrogen bonds between μ3-O2− ions (O1) and the nearest hydrogen atoms of the monodentate carboxylate ligands stabilizes the resulting rigid structure.

The IR spectra of these compounds display a band at 1691 cm−1, assigned to the C⊕O vibration, which confirms the existence of these monodentate ligands.61

The 15 carboxylate ligands (nine bridging Mn ions and six coordinated to the M2+ ions) are surrounding the [MnIV6M2O9]10+ core, and the substituent groups of the benzoate ligands point to the exterior, forming a hydrophobic cage where the metal ions stay isolated from the environment (Figures 1 and S1).

To balance the 10 positive charges of the core, 10 negative charges are needed. Nine of them are compensated with the 4-tBuC6H4COO− bridges. If the six monodentate carboxylate ligands were protonated, a monocharged complex would result and the presence of a counterion in the structure would be required (1:1 electrolyte). However, no counterion was found in these structures. With the aim to confirm the neutrality of these compounds, the molar conductivity of 1 was measured in two different solvents, but these values are much lower than expected for a 1:1 electrolyte, confirming that the compound is neutral. Hence, only five of these monodentate ligands should be protonated. Nevertheless, these ligands are symmetrically equivalent; so, each one contains a hydrogen atom with 5/6 occupancy, consistent with five hydrogen atoms disordered in six identical positions.

Table S2 contains selected structural parameters for 1 and 2. Note that both compounds show almost identical structural parameters, where the most significant differences can be found around the M2+ ions. These differences are commented subsequently. The Mn−O distances are consistent for MnIV ions, without Jahn−Teller axis. Moreover, the oxidation state IV for the Mn ions is confirmed by the magnetic measurements.

The shortest Mn···Mn distances are 2.72 Å (Mn1···Mn2) and correspond to Mn ions linked by two oxo bridges (O1). In contrast, the Mn···Mn distances corresponding to Mn ions linked by one oxo bridge (O2) are 3.27−3.28 Å (Mn1···Mn2a). The Mn1−O1−Mn2 angles are ∼95°, being similar to the values reported in the literature for compounds with [MnIV 2(μ3-O)2(μ-RCOO)]3+ subunits.62 The Mn2O2 ring in 1 and 2 are closer to planarity (with Mn1−O1−O1c−Mn2 angles of ∼172°) than in the discrete dinuclear compounds reported in the literature (159−165°).62

The [MnIV2(μ4-O)(μ-RCOO)2]4+ subunit is uncommon, and to the best of our knowledge, no dinuclear compounds with this core have been reported in the literature. However, we found two theoretical studies in the literature that contain optimized structural parameters for a hypothetical dinuclear [MnIV 2(μ-O)(μ-RCOO)2(NH3)6]4+ complex. In these studies, the Mn−O−Mn angle is expected to range from 126° to 133°.63,64 The Mn1−O2−Mn2a angles in 1 and 2 are within this range, being 127.8° and 130.6°, respectively.

c-Axis views of the packing of 1 and 2 are shown in Figures S4 and S5. Every six molecules form a six-member ring, and such rings share sides, spread out along the a and b axes. The layers are stacked up and extended along the c axis, forming a channel of solvent located in the middle of each six-membered ring.

As explained before, there are not many differences between the structural parameters of 1 and 2, as, for instance, the Mn··· Mn and Mn−O distances vary at most 0.01 Å between the two compounds. However, Sr2+ ion has a larger ionic radii than Ca2+ (1.32 and 1.14 Å, respectively), and this causes slight but key variations in the structural parameters of the wheel. These differences are reflected in the M−O distances and in the respective Ca1···Ca1c and Sr1···Sr1c distances, which are meaningfully

larger in the case of 2 (Sr2+). The wheel diameter (defined by the Mn1···Mn2b distance) may be considered identical because they differ less than 0.02 Å. So as to provide the bigger Sr2+ ion with more space, the Mn2O2 ring of the double oxo bridge becomes more planar (greater Mn1−O1− O1c−Mn2 angle by ∼2°) and the Mn1−O2−Mn2a bridge is slightly unfolded in 2. Lastly, the effect of the greater size of the Sr2+ ion is also reflected with the widening of the unit cell, in light of the larger a, b, and c axes presented by 2.

The structural parameters in 1 and 2 are similar to those found in analogous MnIV 6Mz′x wheels reported in the literature, which contain CeIV or BiIII ions44−46 instead of Ca2+ or Sr2+ ions. However, some slight (but significant) structural differences may be found in both the Mn2O2 and the Mn2O subunits, which may be of importance for their magnetic behavior (see below).

Structural Analysis. As mentioned in the Introduction, the Mn6 wheels can be classified in two types: (a) those where the Mn ions are linked through two oxo or oxo derivatives and (b) those where the Mn ions are alternately bridged by one and two oxo or oxo derivatives. Table S3 summarizes the Mn6 wheels that can be found in the literature so far. Type a compounds are formed by MnII or MnIII ions with one small monovalent or divalent ion in the center, such as MnII, Li+, or Na+, that is usually coplanar or very close to the Mn6 plane (no more than 0.7 Å from it).32−42 It is worth emphasizing that the MnII or mixed-valence MnII/III wheels always show a MnII ion in the center,32−39 while the MnIII6 wheels show alkaline ions (Na+ or Li+).40−42 Type b mainly comprises MnIV6 wheels with one or two large ions in the center,44−46 although a MnIII6 with a MnII ion in the center has been reported.43 It is interesting to note that within the four MnIII 6 wheels reported in the literature,40−43 only one belongs to type b, and in this case, the central ion is MnII instead of the alkaline ions that type a exhibit.

There is a noteworthy dependence of the wheel diameter on the oxidation state of the Mn ions that form the ring; remarkably, the MnIV6 wheels have the smallest diameter (Figure 4). This dependence can easily be rationalized by the Mn−oxo distance decreases, which are shorter for a higher oxidation state and, consequently, lead to a decrease in the wheel diameter.

Regarding type b wheels, it is worth noting that the wheel diameter does not depend on the ionic radii of the central Mz′ but seems to be dictated by the Mn oxidation state, being ∼6.0 Å for MnIV and ∼6.5 Å for MnIII. Moreover, the MnIV6 wheels always have large ions in the center, whose ionic radii range from 1.01 to 1.32 Å. These large Mz′ ions do not fit in the Mn6 plane; thus, they are at 1.5−2.0 Å above it. If a smaller Mz′ ion could be incorporated in a MnIV6 wheel, the M−oxo distances would be shorter and the central ion would tend to be closer to the Mn6 plane. The question arises whether this central ion would possibly fit in the Mn6 plane or would this require a larger ring. We tried to synthesize an analogous MnIV6 compound with Mg2+ as central ions, but the isolated solid did not contain any Mg2+. Hence, the incorporation of a much smaller Mz′ ion such as Mg2+ (whose ionic radii is 0.86 Å) in a MnIV6 wheel could be tentatively considered improbable.

Magnetic Properties. Magnetic susceptibility data were recorded for 1 and 2 from 300 to 2 K. χMT vs T plots are shown in Figure 5. The χMT values at room temperature are 11.3 (for 1) and 10.6 cm3 mol−1 K (for 2), close to the expected value for six uncoupled MnIV ions (11.2 cm3 mol−1 K). For both compounds χMT values decrease as the temperature falls, indicating a net antiferromagnetic behavior, although the more pronounced decline observed for 2 reveals that it presents a stronger antiferromagnetic behavior. χM vs T plots of both compounds (inset in Figure 5) show a maximum at 13 and 30 K for 1 and 2, respectively; below this temperature χM values tend to 0, indicating that the ground state of these compounds is S = 0.

Figure 6 shows the four different Mn···Mn exchange pathways that may be considered to explain the magnetic behavior. The most important magnetic interactions are with the neighbor MnIV ions, J1 and J2 for the [MnIV2(μ3-O)2(μ-RCOO)]3+ and [MnIV2(μ4-O)(μ-RCOO)2]4+ subunits, respectively.

Moreover, there are the magnetic interaction between alternated MnIV ions (J3) and the magnetic interaction between the facing neighbor (J4). The Heisenberg spin Hamiltonian (H) considered is

$$H = J_1 (S_1S_2 + S_3 S_4 + S_5S_6) – J_2 (S_2 S_3 + S_4S_5 + S_1S_6)$$

$$– J_3 (S_1S_3 + S_2S_4 + S_3S_5 + S_4S_6 + S_1S_5 + S_2S_6)$$

$$- J_4 (S_1S_4 + S_2S_5 + S_3S_6) \quad (1)$$

where $S_1 = S_2 = S_3 = S_4 = S_5 = S_6 = 3/2$.

Several fittings of the experimental data were performed, screening different values of the magnetic coupling constants and constraining or omitting some parameters, but we did not succeed to get an appropriate fitting without having good initial values. Therefore, the results of the DFT calculations (presented below) were used to guide the fitting concretely to anticipate the nature and the magnitude of each magnetic coupling. The experimental data were fitted (300−2 K) using the PHI program,65 and with the aim to avoid overparametrization, the g factor was fixed to 2.00. (Note: The Heisenberg spin Hamiltonian in the PHI program is H = −2JS1· S2. However, all J values presented in this manuscript are referred to the spin Hamiltonian H = −JS1·S2, as in eq 1.)

In a first approach, the experimental data were fitted considering J3 and J4 negligible. In spite of obtaining reasonable values of J1 and J2, the theoretical curve did not reproduce properly the shape of the maxima of the χM vs T plots (shown in Figure S6 and in Table 1). Therefore, the inclusion of these parameters seems to be necessary to fit the whole data. Nevertheless, J3 and J4 could not be determined fitting the experimental data because they ended up in abnormal values. We also tried to perform the fit considering J3 = J4 to get an average value, but the obtained values were too high.

Therefore, the experimental curves were fitted with J3 and J4 set to the values of the DFT calculations to better determine J1 and J2 and to avoid overparametrization. The results of the fit are collected in Table 1. As observed, the most important magnetic coupling constants J1 and J2 are of opposite sign, indicating an antiferromagnetic and a ferromagnetic coupling, respectively. This fact was unpredictable and made the fitting very challenging. A survey of the residual between the experimental and the calculated data for different J1 and J2 couples (Figure S7) shows that, for both compounds, the accuracy for J2 values are smaller than for J1 values; hence, small changes of J1 profoundly affect the quality of the fitting.

The diagram of energy levels (shown in Figure S8) calculated with the J values of this latter fit confirms that the ground state is S = 0. This diagram also reveals that the separation between states is greater for 2 than for 1; thus, the ground state is more isolated in 2.

For 1, the magnitude of the ferromagnetic interaction (J2 ≈ + 14 cm−1) is greater than that of the antiferromagnetic one (J1 ≈ −9 cm−1), whereas for 2, with strontium, the magnitude of both interactions is similar (J1 ≈ −18 cm−1 and J2 ≈ + 20 cm−1). Comparison between both compounds shows that the most relevant difference is in the value of the antiferromagnetic interaction J1, stronger for 2 than for 1. This fact could explain the variation in the net magnetic behavior between both compounds. From DFT calculations (see below), J1 and J2 are assigned to the [MnIV 2(μ3-O)2(μ-RCOO)]3+ and [MnIV2(μ4-O)(μ-RCOO)2]4+ subunits, respectively. These results suggest that the magnetic behavior for 1 and 2 is mainly governed by the competition between the magnetic interactions with the adjacent Mn ions (J1 and J2). Consequently, there is spin frustration, as shown in Figure 6.

The J value for the [MnIV2(μ3-O)2(μ-RCOO)]3+ subunit (J1 ≈ −9 cm−1 for 1 and −18 cm−1 for 2) is significantly weaker than expected for this kind of core (from −248 to −73 cm−1),62 probably due to the addition of both structural and electronic perturbations presumably caused by the M2+ ions. On one hand, the attachment of the M2+ ions (located in trans to carboxylate ligand) to the [MnIV2(μ3-O)2(μ-RCOO)]3+ subunits makes the Mn2O2 ring closer to planarity than in discrete dinuclear compounds,62 enlarging the Mn···Mn distance (from ∼2.65 to 2.72 Å) for an identical Mn−O−Mn angle of 95°. On the other hand, there is also a plausible electronic effect of the M2+ ions that may affect the Mn···Mn interaction (see below).

As mentioned before, the [MnIV2(μ4-O)(μ-RCOO)2]4+ subunit is practically unknown, and therefore, there is a shortage of knowledge of its exchange interaction (J2). Nevertheless, there are two theoretical studies reported in the literature for hypothetical [MnIV2(μ-O)(μ-RCOO)2(NH3)6]4+ complexes.63,64 On the basis of these studies, the Mn···Mn interaction for this subunit would be antiferromagnetic. On the contrary, this interaction in 1 and 2 is ferromagnetic (J2 ≈ +14 cm−1 for 1 and +20 cm−1 for 2). The structural differences between this subunit in hypothetical complexes and in these wheels are insufficient to interpret the switch from antiferromagnetic to ferromagnetic interaction.

Several studies have focused their attention on the electronic changes caused by Ca2+ over Mn ions in Mn−Ca cubane-like structures (Mn−Ca2+ WOC and model compounds). The presence of Ca2+ (Lewis acid) modifies the electronic structure of Mn, and this effect is similar to that observed with the protonation of the oxo bridges.24 The same explanation seems to justify the quenching of antiferromagnetic exchange (from −230 to −8 cm−1). Either protonation or attachment of a Lewis acid such as Ca2+ weakens the Mn−O bonds and decreases dramatically their participation in the antiferromagnetic π pathways,64,66 and in some cases a reversal to ferromagnetic coupling is observed.64 With this frame, the attachment of either Ca2+ or Sr2+ (with similar acidities) to the MnIV6 wheel may have an important influence on the Mn···Mn interactions of both Mn2O2 and Mn2O subunits, altering the antiferromagnetic π pathways that dominate these interactions. This influence could be greater for the Mn2O subunit, in which a single oxygen atom with tetrahedral environment interacts with two M2+ ions.

To date, four MnIV wheels with BiIII and CeIV in the center have been reported in the literature,44−46 but the fit of the magnetic data was reported only for the cerium compounds. 44,45 The most relevant structural parameters and the magnetic coupling constant are collected in Table 2. For the Mn2O2 subunit, the most significant differences are found in the Mn−O−Mn angles and in the planarity of the core (Mn−O−O−Mn angle). In both cases, these angles increase with the ionic radii of the Mz′ ions. For the compounds with two central ions (x = 2), J1 switches from a positive value for the cerium compound ←with the greatest z′/r ratio←to the highest negative value for the strontium one (2)←with the smallest z′/r ratio. A similar dependence of the structural and magnetic parameters is observed for the Mn2O subunit. The Mn−O−Mn angle increases with the ionic radii of the Mz′ ion, and with the exception of the compound with only one cerium (x = 1), J2 increases. Thus, the greater the angle is and/or the more voluminous Mz′ ions are, the more ferromagnetic J2 becomes.

Unfortunately, the number of analogous wheels is too scarce to propose a good correlation. However, some points could be remarked: (a) the presence of one or two Mz′ ions could change the magnetic interactions; (b) there is a relation between the Mz′ radii and the wheel's structural parameters; (c) the magnetic properties seem to be correlated with both the structural parameters and the electronic properties of the Mz′, without knowing which is the actual contribution of each one to the Mn···Mn interaction.

Theoretical Calculations. In order to understand the magnetic behavior of 1 and 2, theoretical studies based on DFT calculations were performed. First, the magnetic coupling constants for 1 and 2 from their crystallographic data were calculated. All paramagnetic centers are MnIV, a d3 metal ion in a

pseudooctahedral environment, containing three unpaired electrons. The energy for nine different spin distributions were computed, corresponding to one high-spin and eight low-spin states. Four different coupling constants for these highly symmetric compounds were considered: two alternate J1 and J2 exchange constants for neighboring manganese ions and two others between nonadjacent ones across the alkaline earth ion, J3 and J4. The J values, derived from their computed relative energies, are shown in Table 1. The relative energies for the calculated spin distributions are shown in Table S4.

The calculations for 1 and 2 show an important ferromagnetic interaction for the [Mn2(μ4-O)(μ-RCOO)2]4+ subunit where the MnIV···MnIV distance is around 3.3 Å, being J2 ≈ +28 (1) and +17 cm−1 (2). For the [Mn2(μ4-O)2(μ- RCOO)]3+ subunit (with Mn···Mn distances ≈ 2.7 Å), an antiferromagnetic interaction is found, being J1 ≈ −12 (1) and −30 cm−1 (2). These results are in accordance with the fitting parameters, as they present the same signs and relative magnitudes for J1 and J2.

Up to this point, we have seen that there are substantial differences between the magnetic behavior of 1 (Ca2+) and 2 (Sr2+); the latter presents a stronger net antiferromagnetic behavior. Hence, it seems that there is some effect of the alkaline earth ions, a fact that could be due to the structural dissimilarities between 1 and 2 presented before, to electronic contributions of the M2+ ions or to the addition of the two previous factors. With the aim to provide further insights into the influence of alkaline earth ion over the magnetic behavior, the calculations performed for 1 and 2 were extended to three hypothetical compounds. To do so, we replaced the Ca2+ ions with Mg2+ or Sr2+ and also depleted the Ca2+ ions in the frozen geometry of 1 following the methodology reported by Ruiz et al.58−60 At first glance, it would be desirable to calculate J values with the energies obtained for the optimized geometries. However, small deviations that may occur during the optimization can lead to large changes in the magnetic behavior.58 For this reason, the structural parameters of 1 were used for the hypothetical compounds. As a result, three hypothetical compounds, labeled as Mg2+ model, Sr2+ model, and M2+-absent model, that only differ in the central ions were studied. It should be noted that such calculations just provide qualitative indications, recognizing the limitations of using the structure of 1.60

Comparison of the results obtained for 1 (Ca2+ crystal) and the three hypothetical compounds may provide a further insight into the electronic effects of the M2+ ions, whereas the comparison between Sr2+ model and 2 (Sr2+ crystal) could demonstrate the effect of the structural changes around the MnIV ions.

Table 3 shows the calculated coupling constants for 1, 2, and the three hypothetical compounds. The magnetic coupling constant of the double-oxo bridge (J1) follows the trend: M2+- absent model < Sr2+ model < Ca2+ crystal (1) < Mg2+ model. This trend seems to be correlated with the polarizing character of these ions, which goes from M2+-absent model (no polarizing effect) to Mg2+ (the most polarizing). Similarly, the magnetic interaction of the single oxo bridge (J2) seems to follow the same trend, with the exception of the M2+-absent model. The cause of this divergence could be the electronic environment of the oxo bridge in this subunit, which changes drastically because of the interaction with the two M2+ ions. Structural parameters also appear to be relevant for the magnetic interactions because J1 and J2 values undergo a change when a structural modification is done (from Sr2+ model to Sr2+ crystal (2)).

To illustrate the previous statements, the energy of four spin configurations are represented in Figure 7. As an example, we chose the full ferromagnetic (hs) and the full antiferromagnetic (ls6) configurations, together with the two lowest in energy that contain ferro- and antiferromagnetic contributions (ls7 and ls4). All energies were arbitrarily referred to the full ferromagnetic configuration (hs). As may be noticed, the spin configurations that contain antiferromagnetic contribution (ls6, ls7, and ls4) become more unstable with the polarizing character of the M2+ ions. This theory is consistent with the experimental behaviour of the MnIV6Mz′2 wheels. For instance, the compound with Mz′= CeIV (B in Table 2) shows a net ferromagnetic behavior, according to the high z′/r ratio (3.96 Å−1) of the CeIV ion.

Consistently, 2 (with Sr2+) presents a stronger antiferromagnetic behavior than 1 (with Ca2+), also in agreement with their z′/r ratios (1.52 for Sr2+, 1.75 for Ca2+). Nevertheless, if one relatively compares Ca2+ crystal (1), Sr2+ model, and Sr2+ crystal (2), it may be noticed that a change of ion affects with a similar magnitude than a structural modification does. Hence, the effect of the structural parameters should not be considered negligible.

CONCLUSIONS

Two new heterometallic compounds with formula [MnIV6M2O9(4-tBuC6H4COO)10(4-tBuC6H4COOH)5] have been synthesized with M = Ca2+ and Sr2+. The resolution of their crystal structures revealed that the core of these compounds consists of a planar MnIV6 ring, where Mn ions are alternately bridged by (μ3-O)2(μ-RCOO) and (μ4-O)(μ-RCOO)2 ligands. Two alkaline earth ions (Ca2+ or Sr2+) are located in the center and at both sides of the wheel, linked to the oxo bridges, generating three fused [Mn2M2O4]4+ cuboids. The structural parameters around the Mn ions are affected by the presence of M2+ ions, because they differ from the dinuclear compounds with analogous bridges.

The analysis of the structural data of the Mn6 wheels shows that these compounds could be classified in two groups based on the number of oxo bridges. The diameter of the wheels does not depend on the ionic radii of the Mz′, contrary to one's expectations; however, it depends on the oxidation state of the Mn ions. Furthermore, the formation of MnIV6 wheels seems to be more favorable for large ions than for small ones, such as Mg2+.

The net antiferromagnetic behavior found for these compounds is mostly due to the competition between the ferro- and the antiferromagnetic interactions between adjacent MnIV ions. DFT calculations revealed that the ferromagnetic contribution corresponds to the [Mn2(μ4-O)(μ-RCOO)2]4+ subunit (J2). In spite of the diamagnetic character of the alkaline earth ions, their influence on the magnetic behavior has been evidenced and correlated with their polarizing effect and electron-withdrawing character. Moreover, the magnetic interactions between nonadjacent ions are non-negligible.

AUTHOR INFORMATION

Corresponding Authors

*E-mail: luis.escrichetur@gmail.com.

*E-mail: montse.corbella@qi.ub.es.

Notes

The authors declare no competing financial interest

ACKNOWLEDGEMENTS

This work was supported by the Spanish Dirección General de Investigación (DGI) (projects CTQ2011-23862-C02 and CTQ2012-30662) and the Agenˋ cia de Gestió d'Ajuts Universitaris i de Recerca (AGAUR) of the Generalitat de Catalunya (projects 2009-SGR-1454 and 2009-SGR-1459). L.E. thanks the University of Barcelona for the APIF fellowship. Allocation of computer facilities at IQTCUB and CESCA is also acknowledged.

REFERENCES

(1) Snider, B. B. Chem. Rev. 1996, 96, 339−364.

(2) Yagi, M.; Kaneko, M. Chem. Rev. 2001, 101, 21−36.

(3) Lippard, S. J.; Berg, J. M. Principles of Bioinorganic Chemistry; University Science Books: Mill Valley, CA, 1994. ISBN 0-935702-73-3.

(4) Umena, Y.; Kawakami, K.; Shen, J.-R.; Kamiya, N. Nature 2011, 473, 55−60.

(5) McEvoy, J. P.; Brudvig, G. W. Chem. Rev. 2006, 106, 4455−4483.

(6) Dau, H.; Haumann, M. Coord. Chem. Rev. 2008, 252, 273−295.

(7) Krewald, V.; Retegan, M.; Cox, N.; Messinger, J.; Lubitz, W.; DeBeer, S.; Neese, F.; Pantazis, D. A. Chem. Sci. 2015, 6, 1676−1695.

(8) Askerka, M.; Wang, J.; Brudvig, G. W.; Batista, V. S. Biochemistry 2014, 53, 6860−6862.

(9) Mukhopadhyay, S.; Mandal, S. K.; Bhaduri, S.; Armstrong, W. H. Chem. Rev. 2004, 104, 3981−4026.

(10) Hewitt, I. J.; Tang, J.-K.; Madhu, N. T.; Clérac, R.; Buth, G.; Anson, C. E.; Powell, A. K. Chem. Commun. 2006, 2650−2652.

(11) Jerzykiewicz, L. B.; Utko, J.; Duczmal, M.; Sobota, P. Dalton Trans. 2007, No. 8, 825−826.

(12) Park, Y. J.; Ziller, J. W.; Borovik, A. S. J. Am. Chem. Soc. 2011, 133, 9258−9261.

(13) Kotzabasaki, V.; Siczek, M.; Lis, T.; Milios, C. J. Inorg. Chem. Commun. 2011, 14, 213−216.

(14) Mishra, A.; Wernsdorfer, W.; Abboud, K. A.; Christou, G. Chem. Commun. 2005, 54−56.

(15) Koumousi, E. S.; Mukherjee, S.; Beavers, C. M.; Teat, S. J.; Christou, G.; Stamatatos, T. C. Chem. Commun. 2011, 47, 11128−11130.

(16) Nayak, S.; Nayek, H. P.; Dehnen, S.; Powell, A. K.; Reedijk, J. Dalton Trans. 2011, 40, 2699−2702.

(17) Kanady, J. S.; Tsui, E. Y.; Day, M. W.; Agapie, T. Science 2011, 333, 733−736.

(18) Mukherjee, S.; Stull, J. A.; Yano, J.; Stamatatos, T. C.; Pringouri, K.; Stich, T. A.; Abboud, K. A.; Britt, R. D.; Yachandra, V. K.; Christou, G. Proc. Natl. Acad. Sci. U. S. A. 2012, 109, 2257−2262.

(19) Tsui, E. Y.; Tran, R.; Yano, J.; Agapie, T. Nat. Chem. 2013, 5, 293−299.

(20) Zhang, C.; Chen, C.; Dong, H.; Shen, J.-R.; Dau, H.; Zhao, J. Science 2015, 348, 690−693.

(21) Yocum, C. F. Coord. Chem. Rev. 2008, 252, 296−305.

(22) Yang, J.; Hatakeyama, M.; Ogata, K.; Nakamura, S.; Li, C. J. Phys. Chem. B 2014, 118, 14215−14222.

(23) Polander, B. C.; Barry, B. A. J. Phys. Chem. Lett. 2013, 4, 786−791.

(24) Glatzel, P.; Schroeder, H.; Pushkar, Y.; Boron, T.; Mukherjee, S.; Christou, G.; Pecoraro, V. L.; Messinger, J.; Yachandra, V. K.; Bergmann, U.; Yano, J. Inorg. Chem. 2013, 52, 5642−5644.

(25) Park, Y. J.; Cook, S. A.; Sickerman, N. S.; Sano, Y.; Ziller, J. W.; Borovik, A. S. Chem. Sci. 2013, 4, 717−726.
(26) Tsui, E. Y.; Agapie, T. Proc. Natl. Acad. Sci. U. S. A. 2013, 110, 10084−10088.
(27) Lee, C.-I.; Lakshmi, K. V.; Brudvig, G. W. Biochemistry 2007, 46, 3211−3223.
(28) Pitari, F.; Bovi, D.; Narzi, D.; Guidoni, L. Biochemistry 2015, 54, 5959−5968.
(29) Koua, F. H. M.; Umena, Y.; Kawakami, K.; Shen, J.-R. Proc. Natl. Acad. Sci. U. S. A. 2013, 110, 3889−3894. Inorganic Chemistry Article DOI: 10.1021
(30) Lohmiller, T.; Krewald, V.; Navarro, M. P.; Retegan, M.; Rapatskiy, L.; Nowaczyk, M. M.; Boussac, A.; Neese, F.; Lubitz, W.; Pantazis, D. A.; Cox, N. Phys. Chem. Chem. Phys. 2014, 16, 11877−11892.
(31) Boussac, A.; Rappaport, F.; Carrier, P.; Verbavatz, J.-M.; Gobin, R.; Kirilovsky, D.; Rutherford, A. W.; Sugiura, M. J. Biol. Chem. 2004, 279, 22809−22819.
(32) Langley, S. K.; Chilton, N. F.; Massi, M.; Moubaraki, B.; Berry, K. J.; Murray, K. S. Dalton Trans. 2010, 39, 7236−7249.
(33) Harden, N. C.; Bolcar, M. A.; Wernsdorfer, W.; Abboud, K. A.; Streib, W. E.; Christou, G. Inorg. Chem. 2003, 42, 7067−7076.
(34) Stamatatos, T. C.; Poole, K. M.; Foguet-Albiol, D.; Abboud, K. A.; O'Brien, T. A.; Christou, G. Inorg. Chem. 2008, 47, 6593−6595.
(35) Saalfrank, R. W.; Nakajima, T.; Mooren, N.; Scheurer, A.; Maid, H.; Hampel, F.; Trieflinger, C.; Daub, J. Eur. J. Inorg. Chem. 2005, 2005, 1149−1153.
(36) Koizumi, S.; Nihei, M.; Shiga, T.; Nakano, M.; Nojiri, H.; Bircher, R.; Waldmann, O.; Ochsenbein, S. T.; Güdel, H. U.; Fernandez-Alonso, F.; Oshio, H. Chem. - Eur. J. 2007, 13, 8445−8453.
(37) Koizumi, S.; Nihei, M.; Nakano, M.; Oshio, H. Inorg. Chem. 2005, 44, 1208−1210.
(38) Liu, T.; Wang, B.-W.; Chen, Y.-H.; Wang, Z.-M.; Gao, S. Z. Anorg. Allg. Chem. 2008, 634, 778−783.
(39) Saalfrank, R. W.; Scheurer, A.; Prakash, R.; Heinemann, F. W.; Nakajima, T.; Hampel, F.; Leppin, R.; Pilawa, B.; Rupp, H.; Müller, P. Inorg. Chem. 2007, 46, 1586−1592.
(40) Yang, P.-P. Z. Anorg. Allg. Chem. 2011, 637, 567−571.
(41) Abbati, G. L.; Cornia, A.; Fabretti, A. C.; Caneschi, A.; Gatteschi, D. Inorg. Chem. 1998, 37, 1430−1431.
(42) Yang, P.-P.; Song, H.-B.; Gao, X.-F.; Li, L.-C.; Liao, D.-Z. Cryst. Growth Des. 2009, 9, 4064−4069.
(43) Langley, S. K.; Berry, K. J.; Moubaraki, B.; Murray, K. S. Dalton Trans. 2009, No. 6, 973−982.
(44) Tasiopoulos, A. J.; Milligan, P. L.; Abboud, K. A.; O'Brien, T. A.; Christou, G. Inorg. Chem. 2007, 46, 9678−9691.

(45) Wang, M.; Yuan, D.-Q.; Ma, C.-B.; Yuan, M.-J.; Hu, M.-Q.; Li, N.; Chen, H.; Chen, C.-N.; Liu, Q.-T. Dalton Trans. 2010, 39, 7276−7285.
(46) Stamatatos, T. C.; Oliver, K.; Abboud, K. A.; Christou, G. Inorg. Chem. 2011, 50, 5272−5282.
(47) Sala, T.; Sargent, M. V. J. Chem. Soc., Chem. Commun. 1978, 253−254.
(48) William, J.; Geary. Coord. Chem. Rev. 1971, 7, 81−122.
(49) SADABS, Version 2008/1; Sheldrick, Bruker AXS Inc.: Madison, WI, 2008.
(50) Sheldrick, G. M. Acta Crystallogr., Sect. A: Found. Crystallogr. 2008, 64, 112−122.
(51) Soler, J. M.; Artacho, E.; Gale, J. D.; García, A.; Junquera, J.; Ordejón, P.; Sánchez-Portal, D. J. Phys.: Condens. Matter 2002, 14, 2745.
(52) Perdew, J. P.; Burke, K.; Ernzerhof, M. Phys. Rev. Lett. 1996, 77, 3865−3868.
(53) Kleinman, L.; Bylander, D. M. Phys. Rev. Lett. 1982, 48, 1425−1428.
(54) Troullier, N.; Martins, J. L. Phys. Rev. B: Condens. Matter Mater. Phys. 1991, 43, 1993−2006.
(55) Ruiz, E.; Alvarez, S.; Cano, J.; Polo, V. J. Chem. Phys. 2005, 123, 164110.
(56) Ruiz, E.; Rodríguez-Fortea, A.; Tercero, J.; Cauchy, T.; Massobrio, C. J. Chem. Phys. 2005, 123, 074102.
(57) Ruiz, E.; Alemany, P.; Alvarez, S.; Cano, J. J. Am. Chem. Soc. 1997, 119, 1297−1303.
(58) Ruiz, E.; Alemany, P.; Alvarez, S.; Cano, J. Inorg. Chem. 1997, 36, 3683−3688.
(59) Rodríguez-Fortea, A.; Alemany, P.; Alvarez, S.; Ruiz, E. Inorg. Chem. 2002, 41, 3769−3778.
(60) Ako, A. M.; Burger, B.; Lan, Y.; Mereacre, V.; Clérac, R.; Buth, G.; Gómez-Coca, S.; Ruiz, E.; Anson, C. E.; Powell, A. K. Inorg. Chem. 2013, 52, 5764−5774.
(61) Nakamoto, K. Infrared and Raman Spectra of Inorganic and Coordination Compounds, Theory and Applications in Inorganic Chemistry; John Wiley & Sons: New York, 2008.
(62) Bhaduri, S.; Tasiopoulos, A. J.; Bolcar, M. A.; Abboud, K. A.; Streib, W. E.; Christou, G. Inorg. Chem. 2003, 42, 1483−1492.
(63) Delfs, C. D.; Stranger, R. Inorg. Chem. 2001, 40, 3061−3076.
(64) antazis, D. A.; Krewald, V.; Orio, M.; Neese, F. Dalton Trans. 2010, 39, 4959−4967.
(65) Chilton, N. F.; Anderson, R. P.; Turner, L. D.; Soncini, A.; Murray, K. S. J. Comput. Chem. 2013, 34, 1164−1175.
(66) Krewald, V.; Neese, F.; Pantazis, D. A. J. Am. Chem. Soc. 2013, 135, 5726−5739.
.

630 **Legends to figures**

631

632 **Scheme 1.** Reactions Carried out To Obtain Heterometallic MnIV−M2+ Compounds

633

634 **Figure 1** Crystal structure of 1, with H atoms omitted for clarity. Color code: MnIV, blue; Ca, yellow;
635 O, red; C, gray. The analogous crystal structure of 2 is shown in the Supporting Information (Figure S1)

636

637 **Figure 2.** c-Axis view of the crystal structure of 1. The substituent 4-tBuC6H4− has been omitted for
638 better clarity. An analogous figure for 2 is shown in the Supporting Information (Figure S2).

639

640 **Figure 3** [MnIV6M2O9]10+ core of 1 (Ca2+) and 2 (Sr2+).

641

642 **Fig. 4** Ranges of wheel diameter, defined as the average Mn···Mn distances of the facing neighbor, for
643 wheels with different oxidation states of Mn..

644

645 **Figure 5.** χMT vs T plots and χM vs T (inset) for 1 (red) and 2 (blue); solid line corresponds to the best
646 fit of the experimental data.

647

648 **Figure 6.** Scheme of the possible Mn···Mn exchange pathways in 1 (Ca2+) and 2 (Sr2+). Ranges of
649 Mn···Mn distances for each bridging block are shown in parentheses.

650

651 **Figure 7**. Energetic levels of the different spin states for compounds with a [MnIV6M2O9]10+ core.
652 High-spin states (hs) are arbitrarily taken as zero. (*) Hypothetical isoelectronic compounds using the
653 geometry of 1 but replacing Ca2+ ions with Mg2+ or Sr2+ ones or just removing the Ca2+ ions.

654

655

SCHEME 1

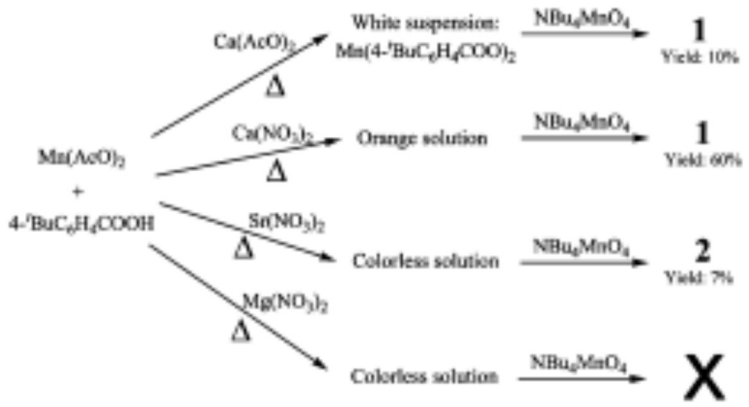
Mn(AcO)2
+
4-tBuC6H4COOH
Ca(AcO)2
Δ
White suspension:
Mn(4-tBuC6H4COO)2
NBu4MnO4
1
Yield: 10%
Ca(NO3)2
Δ
Orange solution
NBu4MnO4
1
Yield: 60%
Sn(NO3)2
Δ
Colorless solution
NBu4MnO4
2
Yield: 7%
Mg(NO3)2
Δ
Colorless solution
NBu4MnO4
X

FIGURE 1

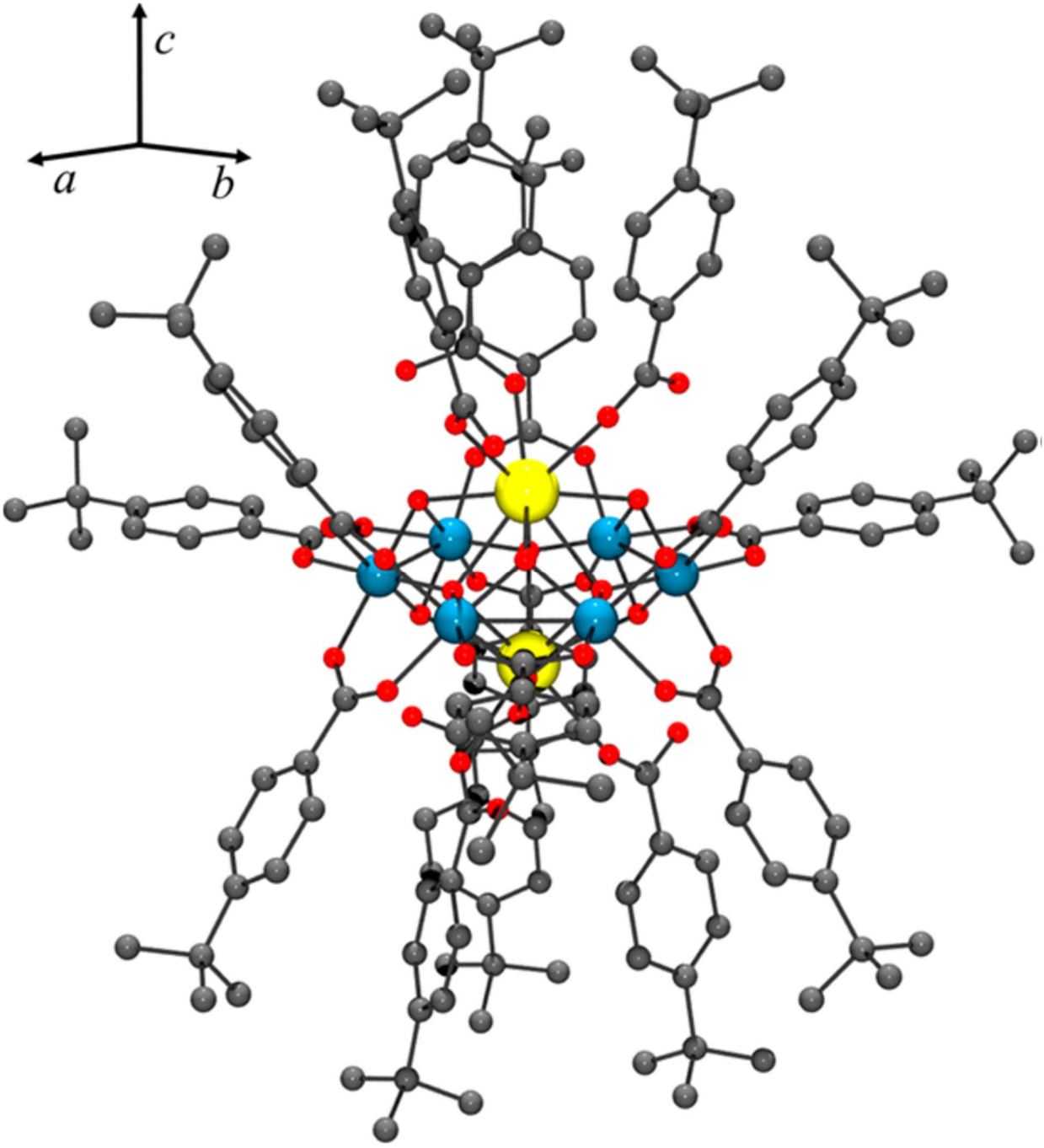

FIGURE 2

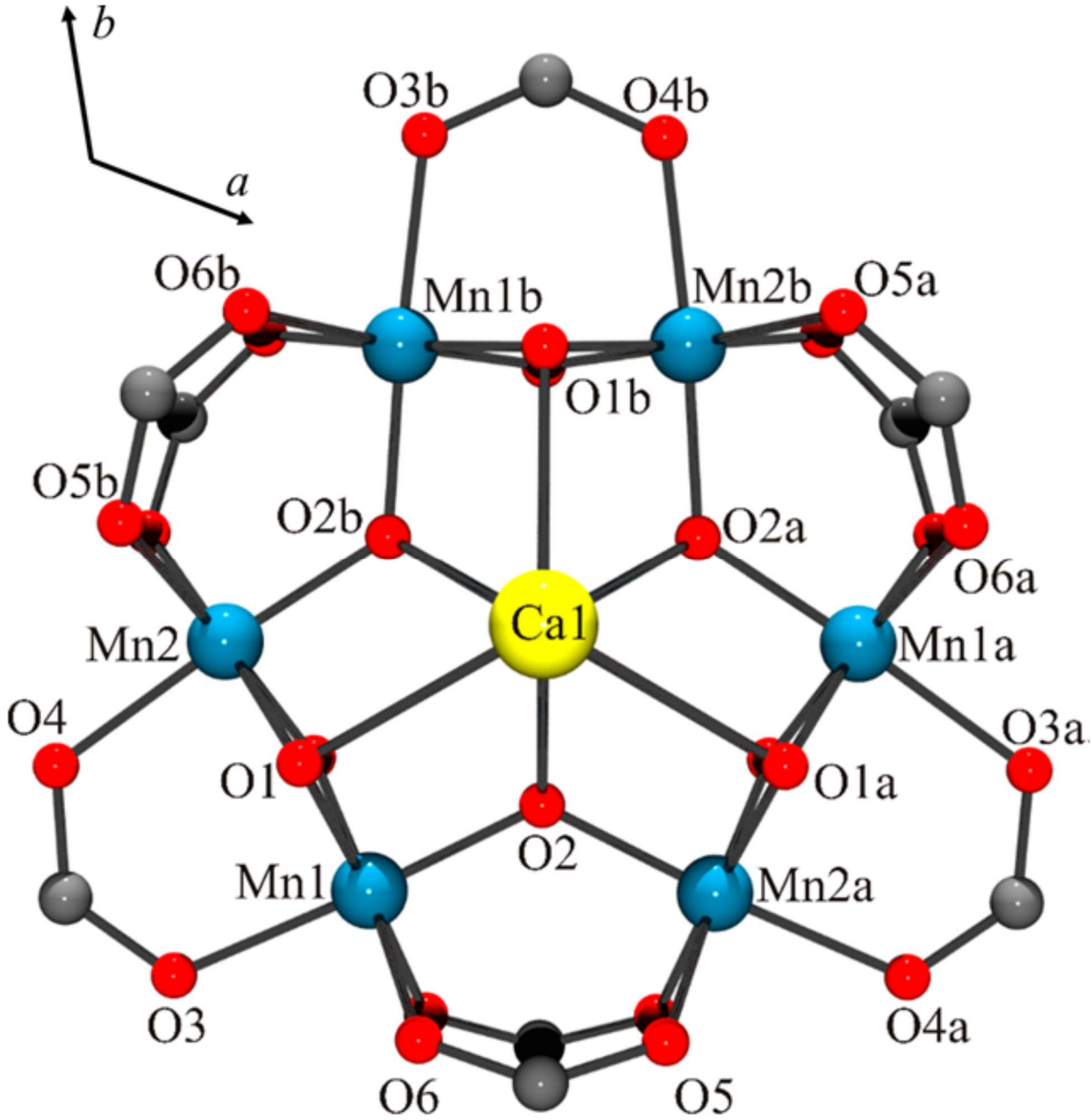
b
a
O3b
O4b
O6b
Mn1b
Mn2b
O5a
O1b
O5b
O2b
O2a
O6a
Ca1
Mn2
Mn1a
O4
O3a
O1
O1a
O2
Mn1
Mn2a
O3
O4a
O6
O5

FIGURE 3

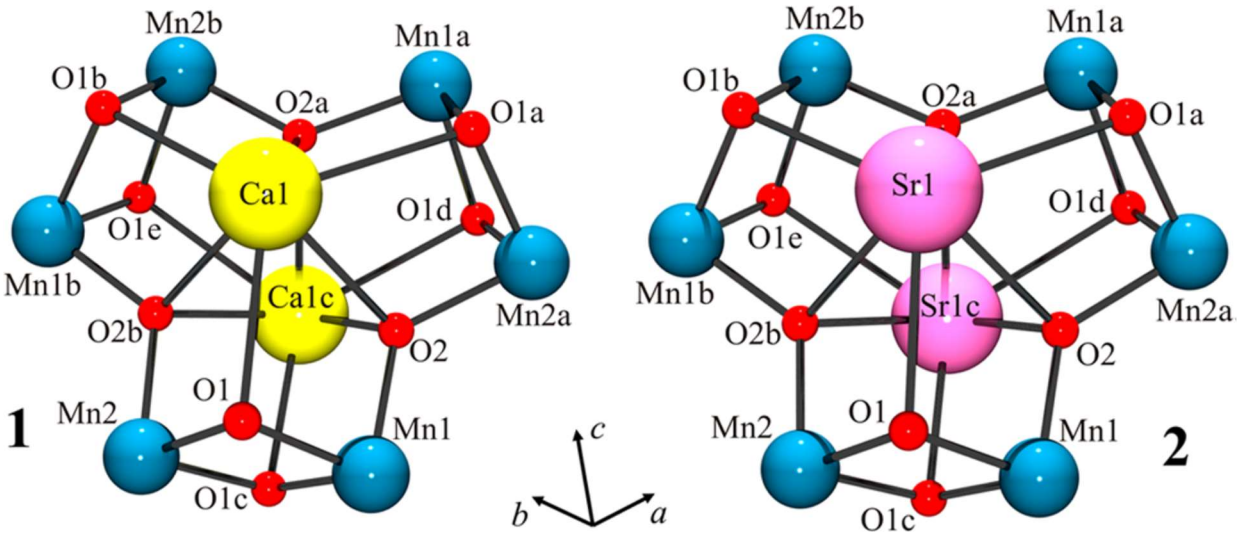
Mn2b
Mn1a
O1b
O2a
O1a
Ca1
O1e
O1d
Mn1b
Ca1c
Mn2a
O2b
O2
O1
Mn2
Mn1
O1c
1
c
b
a
Mn2b
Mn1a
O1b
O2a
O1a
Sr1
O1e
O1d
Mn1b
Sr1c
Mn2a
O2b
O2
Mn2
O1
Mn1
O1c
2

685 **FIGURE 4**

686

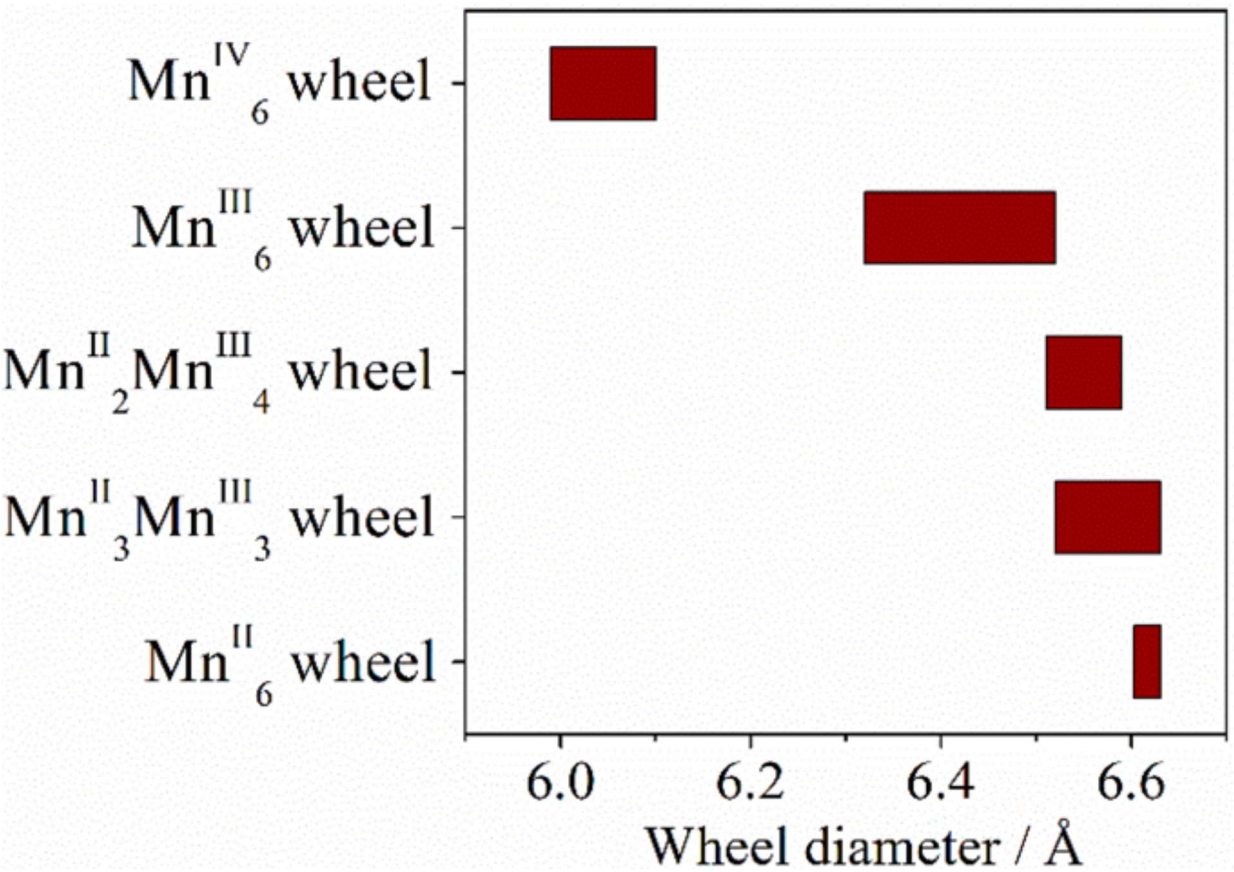

687

688

689

FIGURE 5

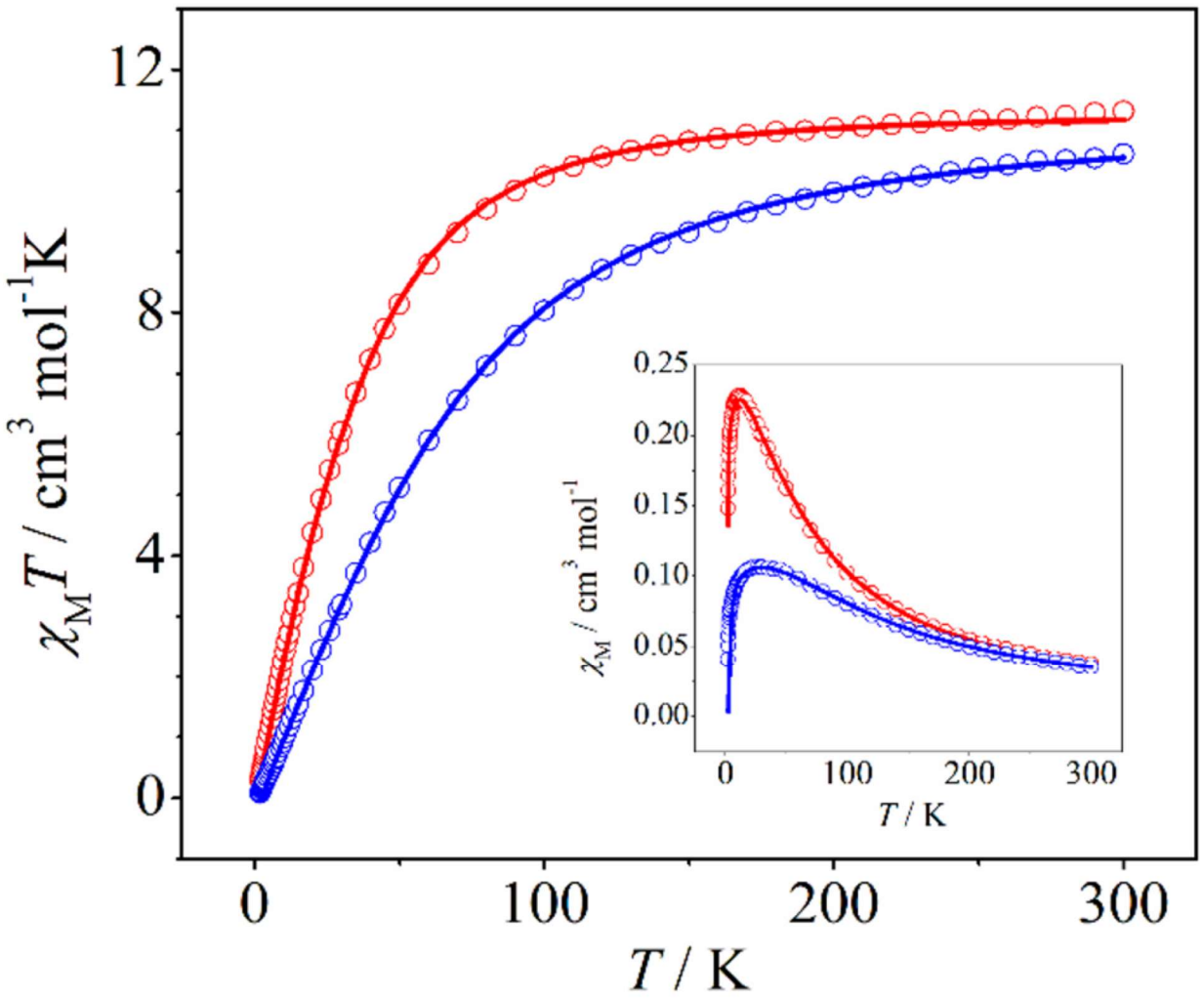
12
8
4
0
$\chi_M T$ / cm^3 mol^{-1}K
0
100
200
300
T / K
0.25
0.20
0.15
0.10
0.05
0.00
χ_M / cm^3 mol^{-1}
0
100
200
300
T / K

FIGURE 6

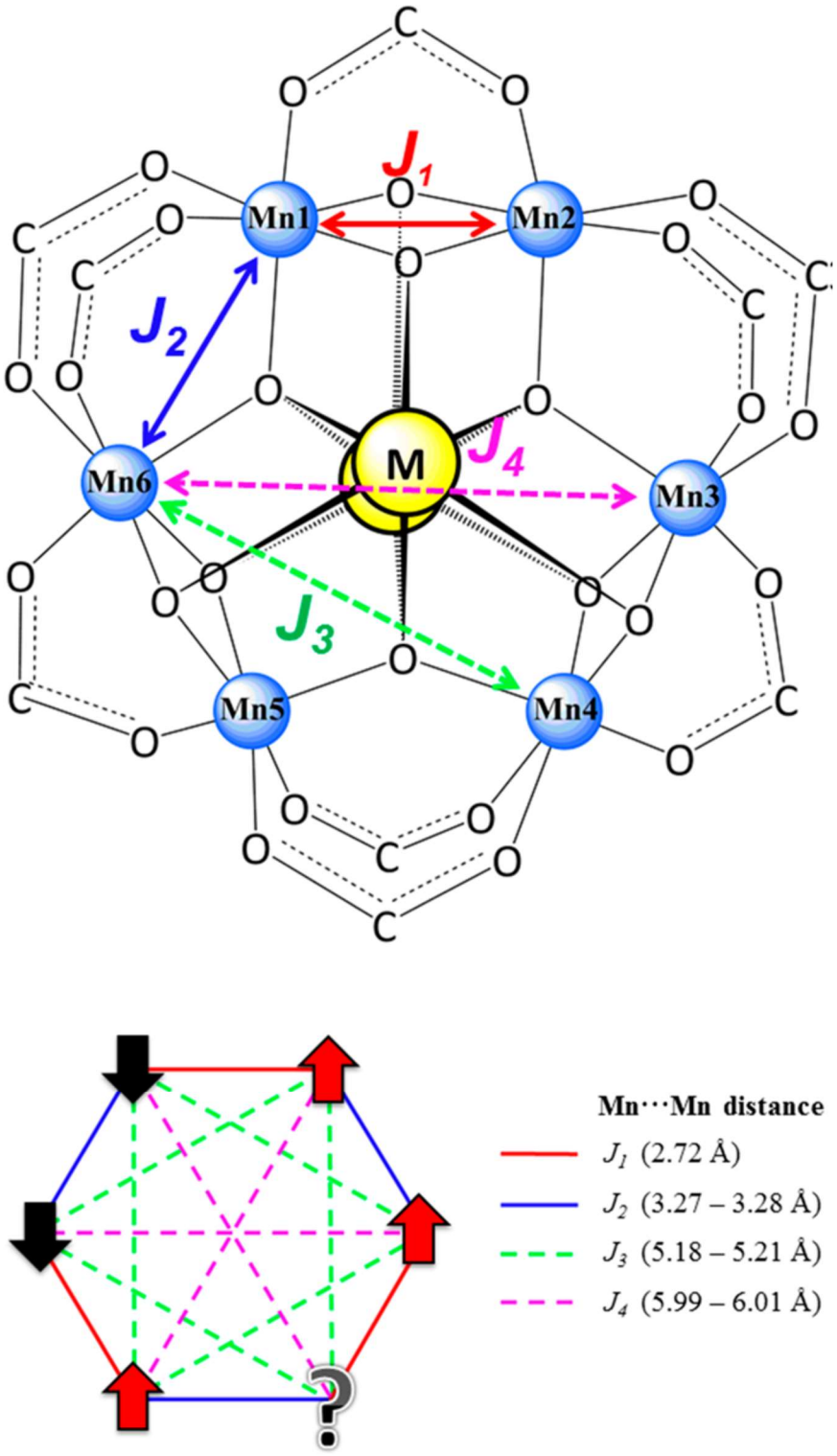
Mn1
Mn2
Mn3
Mn4
Mn5
Mn6
M
J_1
J_2
J_3
J_4
Mn···Mn distance
J_1 (2.72 Å)
J_2 (3.27 – 3.28 Å)
J_3 (5.18 – 5.21 Å)
J_4 (5.99 – 6.01 Å)
?

FIGURE 7

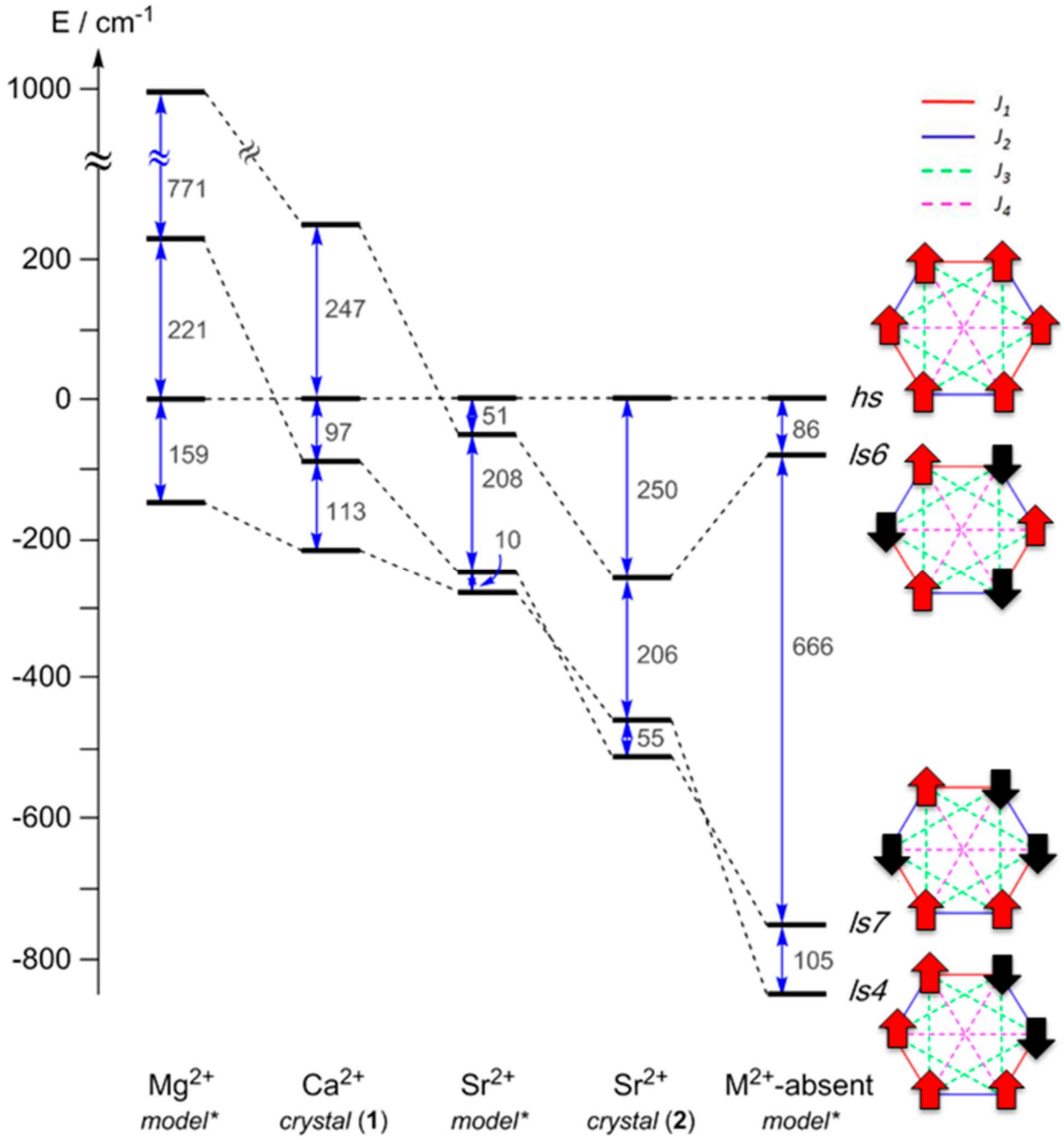
E / cm-1
1000
200
0
-200
-400
-600
-800
771
221
159
247
97
113
51
208
10
250
206
55
86
666
105
J1
J2
J3
J4
hs
ls6
ls7
ls4
Mg2+ model*
Ca2+ crystal (1)
Sr2+ model*
Sr2+ crystal (2)
M2+-absent model*

Table 1. List of Magnetic Coupling Constant from the Fits of χMT vs T Plots for 1 and 2 and Those from DFT Calculations (see Figure 6 for the J scheme)a

	1 (M = Ca^{2+})			2 (M = Sr^{2+})		
J (cm^{-1})	Fit 1	Fit 2	calcd	Fit 1	Fit 2	calcd
J_1	−10.4 ± 0.1	−8.8 ± 0.1	−12.5	−20.3 ± 0.2	−17.5 ± 0.1	−29.7
J_2	+10.5 ± 0.5	+14.4 ± 0.6	+27.8	+13.7 ± 0.7	+19.7 ± 0.5	+17.3
J_3		−1.6[c]	−1.6		−3.5[c]	−3.3
J_4		−1.5[c]	−1.5		−1.3[c]	−1.3
R[b]	5.4×10^{-4}	3.5×10^{-5}		3.8×10^{-4}	3.6×10^{-4}	

[a]Fit 1 considers only two coupling constants with the neighbor ions, and Fit 2 includes four magnetic exchanges incorporating long distance interactions. [b]$R = \Sigma[(\chi_M T)_{exp} - (\chi_M T)_{calcd}]^2 / \Sigma[(\chi_M T)_{exp}]^2$; [c]Taken from the DFT results.

720 **Table 2** Structural Parameters and Magnetic Coupling Constants for MnIV6Mz′x Wheels

721

					$[Mn^{IV}_2(\mu_3\text{-}O)_2(\mu\text{-}RCOO)]^{3+}$ subunit					$[Mn^{IV}_2(\mu_4\text{-}O)(\mu\text{-}RCOO)_2]^{4+}$ subunit			
	$M^{z\prime}$	x	r^a (Å)	z'/r^b ($Å^{-1}$)	Mn···Mn (Å)	Mn–O (Å)	Mn–O–Mn (deg)	Mn–O–O–Mn (deg)	J_1 (cm^{-1})	Mn···Mn (Å)	Mn–O (Å)	Mn–O–Mn (deg)	J_2 (cm^{-1})
A^{4+}	Ce^{IV}	1	1.01	3.96	2.71	1.86; 1.81[c]	93.3; 96.5[c]	169.2	−11.6	3.29	1.83	127.7	−1.2
B^{4+}	Ce^{IV}	2	1.01	3.96	2.70	1.85	93.6	163.7	12.4	3.40	1.91	125.2	+8.3
1	Ca^{2+}	2	1.14	1.75	2.72	1.84	95.22	171.0	−8.8	3.27	1.82	127.9	+14.4
2	Sr^{2+}	2	1.32	1.52	2.72	1.84	95.54	172.9	−17.5	3.28	1.81	130.6	+19.7

[a]Ionic radii of the $M^{z\prime}$ ion. [b]Charge/ionic radii (in Å) ratio of the $M^{z\prime}$ ion. [c]The first one is measured with the oxo ligand linked to the Ce^{IV} ion and the second one with the other oxo ligand. **A**: $[CeMn_6O_9(CH_3COO)_9(MeOH)(H_2O)_3]ClO_4$. **B**: $[Ce_2Mn_6O_6(OH)_3(^tBuPO_3)_6(CH_3COO)_3]$.

722

723

724

Table 3. SelectCalculated Magnetic Coupling Constants (in cm−1) for 1, 2, and the Three Hypothetical Compoundsed Interatomic Distances (Å) and Angles (deg) for Compound 2a

J / cm^{-1}	Sr^{2+} *crystal* (2)	Sr^{2+} *model**	Ca^{2+} *crystal* (1)	Mg^{2+} *model**	M^{2+}-absent *model**
J_1	**–29.7**	**–16.7**	**–12.5**	**+1.6**	**–42.1**
J_2	**+17.3**	**+15.3**	**+27.8**	**+56.5**	**+42.6**
J_3	–3.3	–2.0	–1.6	–5.8	–11.0
J_4	–1.3	–1.4	–1.5	–2.9	–4.8
	← Structural change →		← Change of M^{2+} ion →		

*Hypothetical isoelectronic compounds using the geometry of 1 but replacing Ca^{2+} ions with Mg^{2+} or Sr^{2+} ones or just removing the Ca^{2+} ions.